Interseismic deformation transients and precursory phenomena: Insights from stick-slip experiments with a granular fault zone

M. Rudolf[1], M. Rosenau[1], O. Oncken[1]

[1] *Lithosphere Dynamics, Helmholtz Centre Potsdam, German Research Centre for Geosciences (GFZ), Telegraphenberg, D-14473 Potsdam, Germany*

Corresponding author: Michael Rudolf, michael.rudolf@gfz-potsdam.de

Pre-Print

Please cite as:

Rudolf, M., Rosenau, M., Oncken, O. (2017): Interseismic deformation transients and precursory phenomena: Insights from stick-slip experiments with a granular fault zone. SFB-1114 Preprint in EarthArXiv. pp. 1-27.

Keypoints

- External and internal forcing alter the characteristics of slip events in granular fault analogs
- Precursory slip and transient creep influence predictability of slip events
- A characteristic scale gap between fast and slow slip events is observed

Abstract

The release of stress in the lithosphere along active faults shows a wide range of behaviors spanning several spatial and temporal scales. It ranges from short-term localized slip via aseismic slip transients to long-term distributed slip along large fault zones. A single fault can show several of these behaviors in a complementary manner often synchronized in time or space. To study the multiscale fault slip behavior with a focus on interseismic deformation transients we apply a simplified analog model experiment using a rate-and-state-dependent frictional granular material (glass beads) deformed in a ring shear tester. The analog model is able to show, in a reproducible manner, the full spectrum of natural fault slip behavior including transient creep and slow slip events superimposed on regular stick-slip cycles (analog seismic cycles). Analog fault slip behavior is systematically controlled by extrinsic parameters such as the system stiffness, normal load on the fault, and loading rate. Accordingly, interseismic creep and slow slip events increase quantitatively with decreasing normal load, increasing stiffness and loading rate. We observe two peculiar features in our analog fault model: (1) Absence of transients in the final stage of the stick-slip cycle (”preseismic gap”) and (2) ”scale gaps” separating small interseismic slow (aseismic) events from large (seismic) fast events. Concurrent micromechanical processes, such as dilation, breakdown of force chains and granular packaging affect the frictional properties of the experimental fault zone and control interseismic strengthening and coseismic weakening. Additionally, interseismic creep and slip transients have a strong effect on the predictability of stress drops and recurrence times. Based on the strong kinematic similiarity between our fault analog and natural faults, our observations may set important constraints for time-dependent seismic hazard models along single faults.

1 Introduction

Active faults are characterized by a wide range of slip behaviors ranging from aseismic creep to seismic stick-slip that may change spatially along the fault and temporally over the seismic cycle [e.g. 13, 15]. The types of slip are defined by their characteristic timescale which ranges from milliseconds to a few years [25]. Depending on their characteristics in time and seismic wave forms, the slip events are characterized as seismic (very low frequency earthquakes, tremors, normal earthquake) or geodetic (short-term and long-term slow slip events) events. They can occur simultaneously, i.e. within one seismic cycle, at the same locality or in different depth ranges of the same main fault. The physical origin of this range of slip modes is still not entirely clear, although several valid explanations for certain phenomena have been found. In this study we purely focus on the frictional characteristics of a fault zone which is described within the rate-and-state framework [9, 10]. Other processes that influence the slip modes along a fault zone are variations in pore-fluid pressure, changes in material because of comminution, or mineral reactions. Not all slip modes are observed for all active zones which strongly suggests that there is a complex interaction between the processes acting on different scales in space and time. Knowledge of the complex interactions between the different slip modes is relevant for estimating the seismicity rates along plate boundaries and therefore for seismic hazard assessment.

The rate-and-state framework describes the evolution of sliding resistance, that is friction μ, along an interface between two bodies [9]. Although the friction within geological materials roughly corresponds to the Coulomb friction ($\tau = \mu \cdot \sigma + C$), experiments have shown that friction is not constant and shows a non-linear evolution with sliding velocity, stress evolution and slip history [see 10, and references therein]. This complex evolution of friction generates episodic slip behavior because sliding resistance can decrease once a certain criteria, e.g. sliding velocity, is reached. In very general terms, this can be described by two different friction coefficients. Static friction μ_s that describes the strength of the material at rest and dynamic friction μ_d that describes the sliding resistance in motion. Both terms are used to describe the phenomenological behavior of the system, but both originate from the same heuristic description and continuously evolve during sticking and sliding [9, 32, 26].

The seismic behavior of faults is primarily dependent on its frictional stability which is influenced by several parameters of the fault system [33]. The term stability refers to whether slip can nucleate spontaneously (unstable), only propagate along the interface (conditionally stable), or can not nucleate at all (stable). Stick-slip experiments using rock and rock analogs suggest that besides intrinsic material properties (e.g. friction coefficient, slip/velocity weakening), extrinsic parameters like stiffness, normalized loading rate and effective normal stress are key controls of frictional (in)stability [e.g. 18, 14, 22, 20]. Two types of interfaces are controlling the frictional slip along two crustal blocks. Bare rock surfaces control the slip behavior of young faults, whereas in mature fault zones, the frictional component is mainly defined by fault gouge that forms because of abrasive processes. Both frictional interfaces can exhibit stick-slip type behavior and may evolve over the duration of multiple seismic cycles.

In this study we focus on the effect of a granular material on seismogenesis. We here report characteristics of slip events in an analog fault gouge consisting of spherical glass beads. In contrast to similar experiments [21, 1, 11, 16, 8] we explore the low pressure (kPa instead of MPa) and low stiffness regime which is rich in slip behaviors and generates regular stick-slip with more complete stress drops similar to seismic cycles along major faults in a highly reproducible way. Moreover, the use of a ring-shear tester instead of commonly used direct shear apparatuses allows us to apply an in principle infinite amount of displacement and therefore a large number of events, which is a solid database for statistical analysis.

For the same material we vary the extrinsic parameters normal stress σ_N, loading velocity v_L, and stiffness k_L. In this parameter space, we monitor the occurrence of slip events and creep, as well as the transitions from one slip mode to another. The main purpose of this study is to demonstrate the influence of interseismic transient slip phenomena on the overall seismic cycle behavior. We compare the findings to first order observations from earthquake catalogs and to rock friction experiments.

2 Methods

2.1 Setup

For the experiments we use the ring shear tester of type 'RST-01.pc' [34] with slight modifications (additional spring to reduce the stiffness). As a fault gouge analog material we use 300-400 μm sized fused quartz microbeads (Figure 1c). They are characterized by a relatively low friction coefficient (ca. 0.5) and cohesion (10-40 Pa) as well as a strain hardening-weakening behavior associated with dilation-compaction [19, 17, 27]. They are frequently used as a rock and gouge analogue material and generate stick-slip under laboratory conditions [e.g. 20]. In our setup, the glass beads are confined in a ring shaped shear cell and sheared against a lamellae-casted lid which also imposes the normal load (Figure 1a+b). Two bars attached to force transducers hold the lid in place. A granular shear zone of a few millimeters thickness localizes at the base of the lamellae. The applied and resulting forces (normal and shear), driving velocity (v_L, measured along a diameter dividing the cell area into two equally sized compartments) and vertical lid displacement (dilation d) are measured at a frequency of 12.5 kHz each.

All measured values are averaged over 20 samples for noise reduction resulting in a final output frequency of 625 Hz, high enough to study the stick-slip events at high resolution. Based on the setup geometry, we convert shear and normal forces into shear and normal stresses and lid displacement into volumetric change (dilation/compaction). Instead of displaying shear stress, we use the dimensionless actual friction (coefficient) μ which is defined as the shear force divided by the normal force throughout the manuscript.

Before an experiment is started, the sieved samples are presheared by 10 mm which ensures a fully developed shear zone without major post failure weakening [derived from 27, 28]. The experiments are conducted as velocity stepping tests with logarithmically decreasing loading velocity V_L from $5{\cdot}10^{-2}\ \frac{mm}{s}$ to $8{\cdot}10^{-4}\ \frac{mm}{s}$. Normal stress σ_N is fixed for each individual time series. We use 4 different normal stresses of 5, 10, 15, and 20 kPa. For each velocity step the amount of displacement is constant, which leads to an approximately equal number of events per velocity step.

Previous studies examined granular media under natural pressure conditions, whereas we are using conditions realized by analog models, being 3 - 4 orders of magnitude lower [29]. This

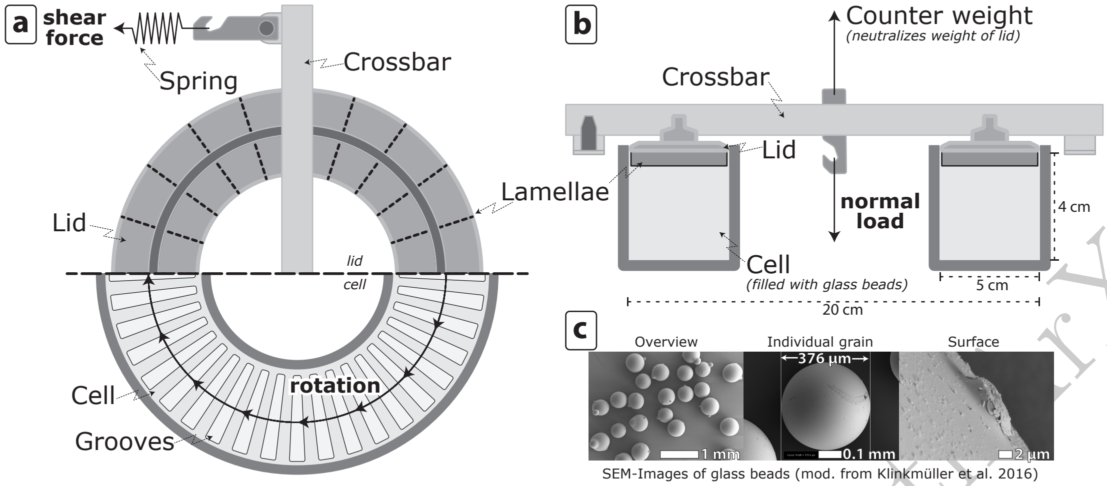

Figure 1: Schematic drawing of the modified ring shear tester. The system is loaded at loading velocities of $5{\cdot}10^{-2}$ to $8{\cdot}10^{-4}$ $\frac{mm}{s}$ by rotating the cell. The cell has grooves for a high friction interface which is mirrored by lamellae attached to the lid. A moveable weight pulls the lid from below by a motor driven lever for applying normal load. Force transducers behind the springs measure shear force. a) Top view the above part showing the lid and the bottom part showing the cell and its internal structure. b) Crosssection through the whole setup. c) Scanning electron microscopy images of the glassbeads showing the average particle size and the surface structures [modified from 17].

prevents comminution of the glass beads and ensures constant frictional properties over the experimental duration, which gives well reproducible results.

2.2 Stiffness of the system

Three different types of stiffness are relevant for our setup. The loading stiffness k_L that is defined by the combined stiffness of the testing apparatus, force transducers, and attached spring without sample material. Loading stiffness changes from 1335 $\frac{N}{mm}$ (without spring) to 20 $\frac{N}{mm}$ (with spring). The unloading stiffness k_u which relates the stress drop to lid displacement during an event. It is measured for both setups (with and without spring) at all experimental normal stresses. Without spring the unloading stiffness is 624 $\frac{N}{mm}$, whereas with the spring it is 18 $\frac{N}{mm}$. The third stiffness acting in the system is the effective cyclic reloading stiffness k_c which includes the machine, spring and the material. It is derived from the linear fit of stress increase during the first 40% of the interseismic phase. This reloading stiffness is also used to calculate creep during the interseismic phase. For creep estimation, the linear trend is extrapolated to the point of failure and related to the measured stress at failure. For experiments without a spring k_c is 503 to 578 $\frac{N}{mm}$ and increases with normal stress. In contrast, k_c with a spring is very similar for normal stresses of 10 kPa and above, namely 33 to 34 $\frac{N}{mm}$, whereas for 5 kPa the stiffness doubles and is 67 $\frac{N}{mm}$.

2.3 Loading velocities

For a better comparison with other studies we normalize the loading velocity by cyclic reloading stiffness k_c and by normal stress σ_N to obtain a normalized loading rate $\dot{\mu}$. It describes the increase in non-dimensional frictional stress in the glass beads per second:

$$\dot{\mu} = \frac{V_L k_c}{\sigma_N} \tag{1}$$

In the presented experiments, normalized loading rates cover five orders of magnitude, with some overlap between experiments with and without spring. They range from 10^{-5} to 10^{0} s^{-1} which is comparable to experiments that have been conducted with rock samples in a geometrically similar apparatus at Brown University but with stress levels in the MPa-range [37, 3]. Other experiments at very low normal stresses of less than 100 Pa that have been performed by **(author?)** [24, 23] and are in the range of 10^{-3} to 1 s^{-1} but with a geometrically different setup (pure spring-slider).

2.4 Data Analysis and Processing

The acquired measurements are analyzed with a suite of MATLAB scripts. Each slip event is automatically picked using two methods. The first method picks each event with a very simple peak-detection algorithm that compares each point with its neighbours. If a critical height or low is reached, the point is detected as either start or end of a slip event. For each experiment this threshold is adjusted to minimize the amount of wrong detections and varies between 10 and 45 Pa. Some experiments show slip events which have a strongly differing stress drop rate $\dot{\tau}$. A fast slip event is detected when a critical stress drop rate, a proxy for slip velocity, is reached. This may differ from experiment to experiment, and also depends on loading velocity, and is therefore manually picked for each time series. It varies between -620 $\frac{Pa}{s}$ and -7273 $\frac{Pa}{s}$. The experimental data, parameters, and scripts for reproducing the figures in this study can be found in **(author?)** [31].

2.5 Assessing Predictability

As the regular stick-slip serves as an analogue for seismic cycles along major faults in nature we test for time and slip predictability and assess how interseismic transients affect the predictions. Time predictability is assessed after **(author?)** [5] which relates previous stress drop with stressing rate to predict the time until the next event:

$$t_r = \frac{\Delta\tau_{t-1}}{V_L k_c} \tag{2}$$

Slip predictability is assessed following **(author?)** [36] which calculates the expected stress drop $\Delta\tau_{t+1}$ by relating time passed since the previous event t_r and stressing rate:

$$\Delta\tau_{t+1} = t_r V_L k_c \tag{3}$$

To quantify the accuracy of both predictions the mean forecast error e_n is calculated and normalized by the measured mean $\bar{x}$. It is defined as the average difference of the predictions to the observations, divided by the mean of the measurements:

$$e_n = \frac{\frac{1}{n}\sum_{i=1}^{n}(x_{measured} - x_{predicted})}{\bar{x}} \tag{4}$$

The resulting values for e_n indicate how predictions differ from the measured values. If $e_n < 0$ the model tends to over forecast the observations and if $e_n > 0$ the model under forecasts the observations. For $e_n = 0$ model and observation are equal. The absolute value shows by how much the model is inaccurate normalized to the observation mean.

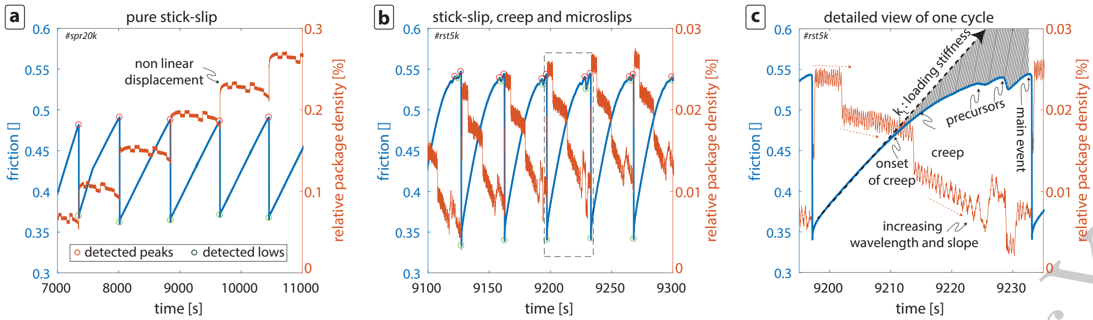

Figure 2: Typical stick-slip curves generated by the setup. Shear stress is normalized by normal load and shown in blue. Lid displacement (15 Hz low pass filtered), here relative to the lowest y-axis point for comparison, is shown in orange. Results of the peak detection is shown as red and green colored circles. (a) Experiment with low stiffness (spring) with few but relatively large events in a sawtooth shape. (b) High stiffness test (no spring) at the same velocity as in Figure 2a. The event rate is higher, with precursors and creep. (c) Detailed view of one cycle from Figure 2. After the previous slip event (t_{i-1}) with a slight overshoot, the system is reloaded linearly. In the second half of the cycle the fault zone starts to creep and finally shows several slow precursory events. Finally a new main event (t_i) occurs and stress drops to a similar level as for t_{-1}.

3 Observations

3.1 Stick-slip cycles

The glass beads show cyclic increases in shear stress followed by sudden stress drops characteristic for stick-slip. Because stick-slip is an analogue for seismic cycles we here use co- and interseismic as synonyms for the slip and stick (or locking) phase. For experiments with low loading stiffness (with spring, #spr..k) the stress-time evolution closely follows a sawtooth shaped curve with linear increases indicative of full sticking during the loading phase (Figure 2a). For higher loading stiffness (without spring, #rst..k) and at low normal stress, the loading curves become increasingly non-linear at higher stresses indicating accelerating interseismic creep (Figure 2b). In addition, smaller and slower slip events emerge close to failure stress and in the last third of a cycle of stiff systems.

Stick-slip cycles are associated with systematic volume changes: Interseismic dilation and coseismic compaction in the order of of 0.025 to 0.050 %. Interseismic dilation is non-linear and accelerates towards failure, in particular for the stiff system. Additionally, the lid displacement shows several distinct upward and downward steps of 1-2 μm which are not necessarily mirrored in the stress curve but very repetitive and similar for each interseismic phase. Another, second order, observation is that the low amplitude oscillations in the low pass filtered signal show an increase in their wavelength towards the end of the interseismic phase (Figure 2c). A secular trend over the experiment run indicates progressive material loss through the small gap between lid and shear cell.

The slip events show a characteristic size distribution which is unimodal for low stiffness and bimodal for high stiffness (Figure 3a+b). At low stiffness the distributions show a log-normal character with a positive skew. A comparison using Q-Q plots shows that all distributions are similar, except the distribution for the experiment at low normal stress of 5 kPa which has a slightly different shape and is shifted towards smaller sizes. The median is $\approx$0.036, while all other distributions show a significantly higher median of $\approx$0.066.

For a high stiffness the distributions are bimodal with one mode at very low stress drops <0.05 and one mode at higher stress drops. All events that belong to the lower mode are considered as precursors because of their lower stress drop rate compared to the catastrophic failures defining the higher stick-slip cycles (shaded area in Figure 3b). When the events are separated into precursors and main events each of the respective populations are similarly normal distributed. The median size of the precursors is $\approx$0.005 and $\approx$0.169 for the main events. Likewise, the experiment at a normal stress of 5 kPa is somewhat different from the other experiments. Although the median value does not show a significant difference, the distribution of the main events is broader and does in itself show a weak bimodal characteristic.

3.2 Precursory slip events

For the high stiffness setup small scale interseismic (precursory) small slip events can be detected. They are characterized by low stress drop and low stress drop rate. The relative amount of precursors decreases with increasing normal stress. For low normal stress more than 40% of the detected events are found to be precursors, whereas for higher normal stresses it is 5 - 10%. Additionally, there is a variation in occurrence with loading velocity. At high loading velocity only very few precursors are detected, while at low loading velocity multiple precursors of increasing size can occur before one main event.

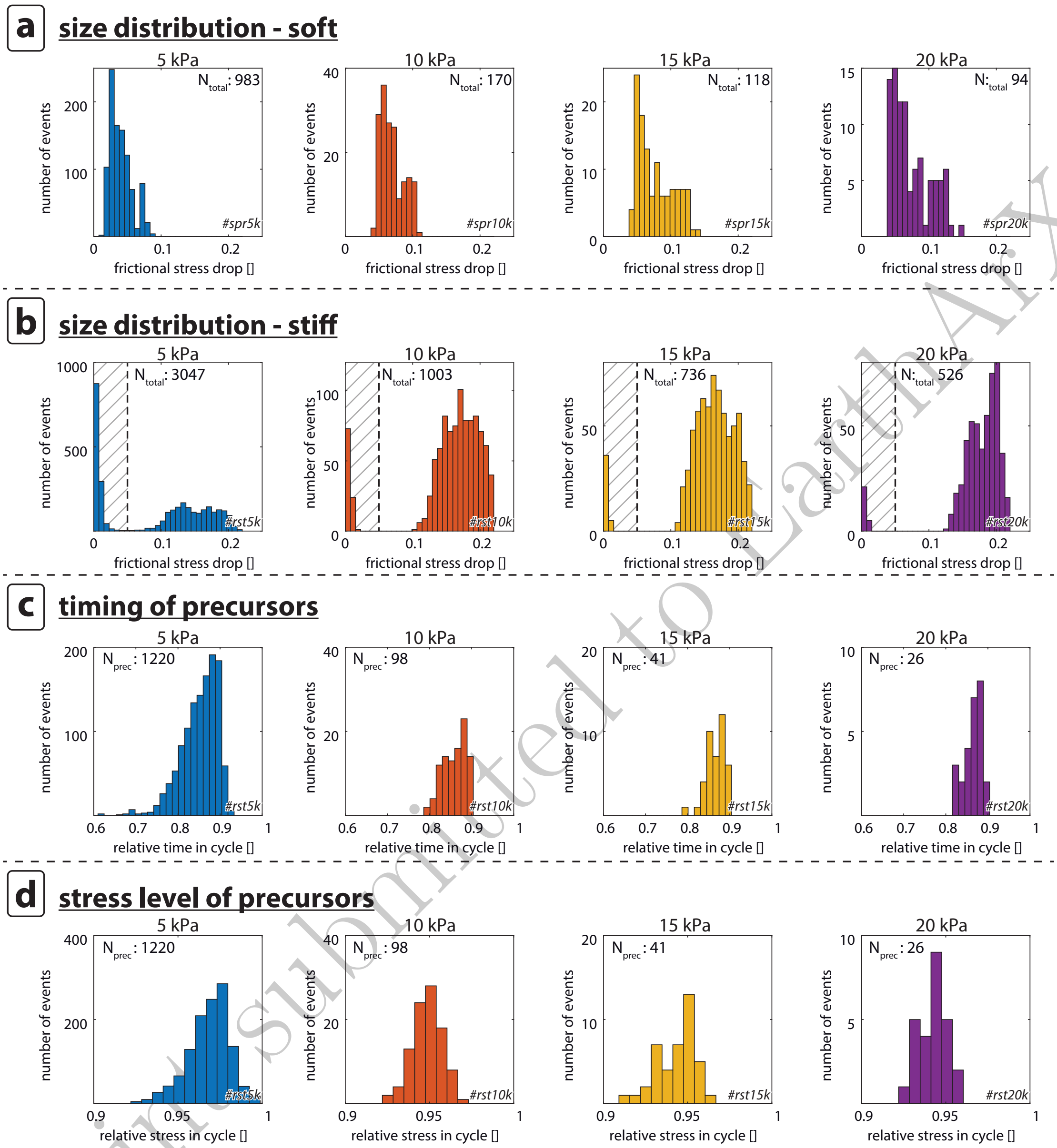

Figure 3: Distributions of event size and precusor occurrence. (a) Size distributions of slip events with spring (low stiffness). All distributions show a slight log-normal trend. (b) Size distribution for experiments without spring (high stiffness). The shaded area shows the location of the precursory events. (c) Timing of the precursor events within an event cycle. All precursors occur in the second half of the cycle and show an increased occurrence towards the end. (d) Stress level at which the precursors occur in the event cyle. They mainly happen at stresses close to failure ($>0.9\tau_f$) with a slightly decreasing median with increasing normal stress.

In terms of frictional stress drop, most precursory slip events are at least one order of magnitude smaller than the main events. The average stress drop of a precursor is only 2.6% of the corresponding main event.

The occurrence of precursors shows a specific temporal pattern. They do not occur in the first half of the interseismic cycle. The probability of occurrence increases between 0.7 and $0.9t_r$ and peaks at $\approx 0.85t_r$ (Figure 3c). Then the probability drops abruptly to zero and for all experiments almost no precursor has been detected in the last 10% of the interseismic cycle. The stress level at which the precursors occur is generally very close to the stress level of the main event (Figure 3d). For higher normal stresses the precursors occur around $0.95\tau_f$, and for σ_N =5 kPa at higher stresses of $0.97\tau_f$. Few events happen at stresses equal to the stress level of the main events.

3.3 Event scaling

In the parameters space tested, we observe distinct systematics and gaps in the spectrum of observed slip rates. All events show an increase in stress drop rate with increasing loading rate (Figure 4a+b). This increase is independent of the amount of total stress drop, although a high stress drop coincides with a higher stress drop rate. For low stiffness experiments the events for 10 kPa and above fall into one category that show an increase in stress drop rate with loading rate of $\frac{\Delta\mu}{\Delta t} \propto \dot{\mu}^{0.36}$. For the low normal stress experiment the scaling is similar, but the whole cluster is shifted to higher normalized loading rates.

At high stiffness three clusters are observed that show different characteristics (Figure 4b). One cluster contains all precursor events that show low stress drop and low stress drop rates (shaded area in Figure 4b). They scale much stronger with loading rate and show an increase in stress drop rate by $\frac{\Delta\mu}{\Delta t} \propto \dot{\mu}^{0.87}$. A second cluster shows a scaling similar to the events at low stiffness with $\frac{\Delta\mu}{\Delta t} \propto \dot{\mu}^{0.46}$. But here the stress drop increases more strongly with decreasing loading rate than for low stiffness. A small cluster of very fast (>2s^{-1}) and large ($\Delta\mu$ >0.2) events is also observed (upper rectangle in Figure 4b). At the highest loading rates main events and precursors form a more continous distribution and are only separated by the difference in stress drop.

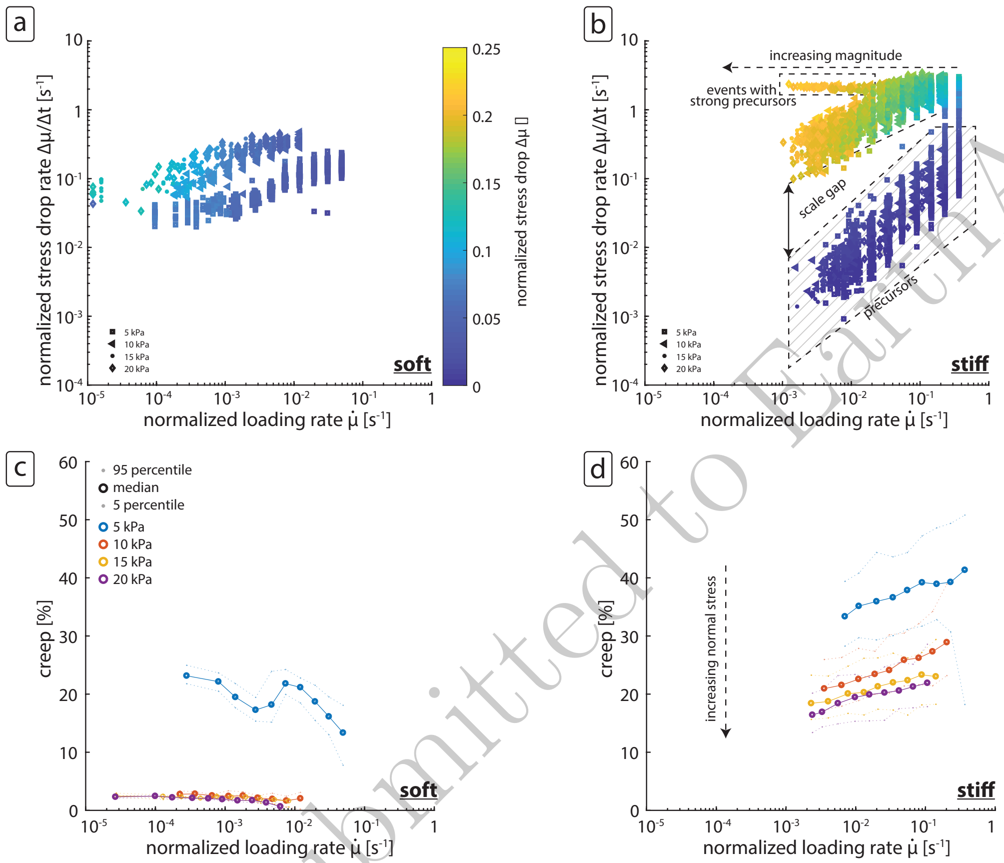

Figure 4: Scaling behavior and creep during the experiments. (a) Comparison of normalized stress drop rate and loading velocity for low stiffness. All detected events fall into a cluster of similar stress drop rate at each loading velocity. (b) Experiment with high stiffness where the precursors form a separate cluster (shaded area). They show significantly reduced stress drop rates and are much smaller. (c) Amount of creep as a function of normalized loading rate and normal stress for low experimental stiffness. Significant creep is only occurring at very low normal stress. (d) At high stiffness all experiments show creep, which decreases with increasing normal stress and decreasing normalized loading rate.

3.4 Creep

Each main slip event is followed by an initial phase of linear elastic loading indicating full postseismic locking. For experiments with high stiffness (#rst..k) and low load (#spr5k) this linear loading transitions into a non-linear loading phase. The amount of creep is derived by calculating the theoretical failure stress at the observed time of failure by linear extrapolation of the cyclic reloading stiffness, and estimating the stress deficit at the point of failure. This stress deficit is balanced by the total amount of interseismic deformation, including precursors, that has been released during each cycle. Accordingly, some precursory slip events can account for more than 30% of creep deformation but on average they only account for 10% of total interseismic creep.

The amount of creep is depending on the loading rate and on normal stress (Figure 4c+d). An increase in normal stress leads to a strong reduction of creep and high stiffness experiments indicate that creep slowly approaches a non-zero limit (Figure 4d), rather than dropping to values near zero as is observed for the low stiffness experiments (Figure 4c). Furthermore, for high stiffness the total amount of creep increases with increasing loading rate but also the variability of creep per event increases.

4 Discussion and Interpretation

4.1 Micromechanical processes

Granular material gains shear strength due to force chains oriented in the direction of the maximum stress [6]. Depending on the number, length and orientation distribution of such chains shear deformation might be stable or unstable. Stick-slip is therefore interpreted as a cyclic setup and breakdown of force chains, the frequency and size of which should be a function of grain size distribution [20]. Furthermore, granular materials exhibit so called 'jammed states', where jamming is induced at high packaging density or by application of shear stress [4]. We corroborate this view as large slip events are associated with compaction while the interseismic is characterized by accelerating creep and dilation (Figure 2).

The normal stress is one of the critical factors that control the creep threshold of the system.

For low normal stresses it is easier for the grains to rearrange during the creep phase. Firstly, this results in higher background slip of grains that exhibit a much lower normal stress along their contacts and can easily slide along each other. Secondly, the ratio of normal stress to dilational stress, that pushes the grains apart when sliding over the rough internal shear zone, is smaller. Therefore, force chains are less effective in strengthening the material.

The occurrence of small precursory slip events is in accordance with other studies that show transient effects during the transition of the stick phase to dynamic slip [23, 11]. Because they are much smaller than the main events it is suggested that the events are the expression of internal reorganization in the granular material. During this internal deformation the grains are jammed and the force chains are rearranged into a more stable configuration. Although creep continues the newly formed granular package is stronger than the previous package and therefore a short period of quiescence without slip events occurs. This rearrangement can occur several times during the late interseismic phase. If the internal structure reaches a critical threshold, probably determined by the contact ratio and packing density, a runoff process starts and the system changes from creeping to dynamical slip.

The behavior of dilation during the interseismic cycle is even more complex and it is difficult to assign a direct relation to micromechanical processes. The observed increase in wavelength of the small amplitude oscillations could indicate a smoothing of the internal fault surface, leading to a smoother frictional response. The discrete upward and downward steps might be artificial, or the result of sensor noise. However, the strong reproducibility over multiple cycles indicates that mechanical explanations can be valid, too. For example, internal reorganization of the granular packaging leads to discrete conformations of packaging with different densities that are characteristic for each state of the system.

4.2 Effect of creep on rate and state relations

We test if interseismic transients have an effect on the rate and state relations that can be determined by looking at the velocity and time dependence of friction during each experimental series. In rate and state friction three key parameters are determined, the direct effect a, the healing effect b, and the state evolution variable ϕ [9, 22]. From our type of experiments we can not observe the evolution of friction directly because our system is inherently unstable. This is due to the system stiffness k_L which is below the critical stiffness k_c. Therefore we can only infer the amount of weakening depending on loading velocity $(a-b)$ and the relation of loading velocity and recurrence time $V_L = C\, t_r^n$ [equation (5) in 2].

The main events show typical scaling of peak strength μ_p with loading velocity V_L. From this the rate-and-state parameter $(a-b)$ is derived because peak strength is the onset of dynamical failure and at that point the slip velocity V equals the loading velocity V_L [29]. We fit the curve with a power law of the form $\mu_p \propto V_L^n$ with $n = (a-b)ln(10)$ (figure 5a+c). This shows that the glass beads are velocity weakening with $(a-b)$ ranging from -0.011 to -0.017 which leads to a reduction of peak strength by 1.1 to 1.7 % per e-fold increase in velocity.

There is no significant difference in the estimate of $(a-b)$ from soft and stiff systems, as expected for a material property. The scaling of strength at the onset of slip is consistent with the findings of **(author?)** [2] who show the same type of scaling. The scaling coefficient typically attributed to natural rocks or gouge in the seismogenic zone, is in the same range (-0.011 to -0.015 [2]; ≈-0.01 [33]; -0.001 to -0.01 [10]). Other analog model studies have used $(a-b)$ values in the same range to model seismotectonic processes with other materials (gel on sand paper: -0.028 [7]; rice: -0.015 [30]; cacao, ground coffee, and others: [29]). Therefore, we consider our models to be dynamically similar to the natural prototype, to rock deformation experiments in the MPa-range [e.g. 37], and to numerical simulations of rate and state friction [e.g. 11].

Usually, slide-hold-slide tests are used to determine the healing effect b which scales as $\Delta\tau_p \propto bln(t_h)$, showing that with increasing hold time t_h the strength of the material is increasing. As described in section 3.1, the interseismic creep and precursors strongly affect the recurrence behavior of main events, essentially making them not predictable by classical laws of predictability. Due to the interseismic deformation the fault zone is not at complete rest, which would be the case for a stress relaxed slide-hold-slide test.

According to **(author?)** [2] if time-dependent strengthening is present the scaling relation of loading velocity and recurrence time $t_r \propto V_l^n$ shows an exponent $n > -1$. For the stiff experiments n is between -0.981 and -0.943 which shows that a time-dependent healing effect leads to a strengthening of the fault zone over the recurrence interval (Figure 5c). So what is a possible source of time-dependent strengthening in our system? To some extend interaction on

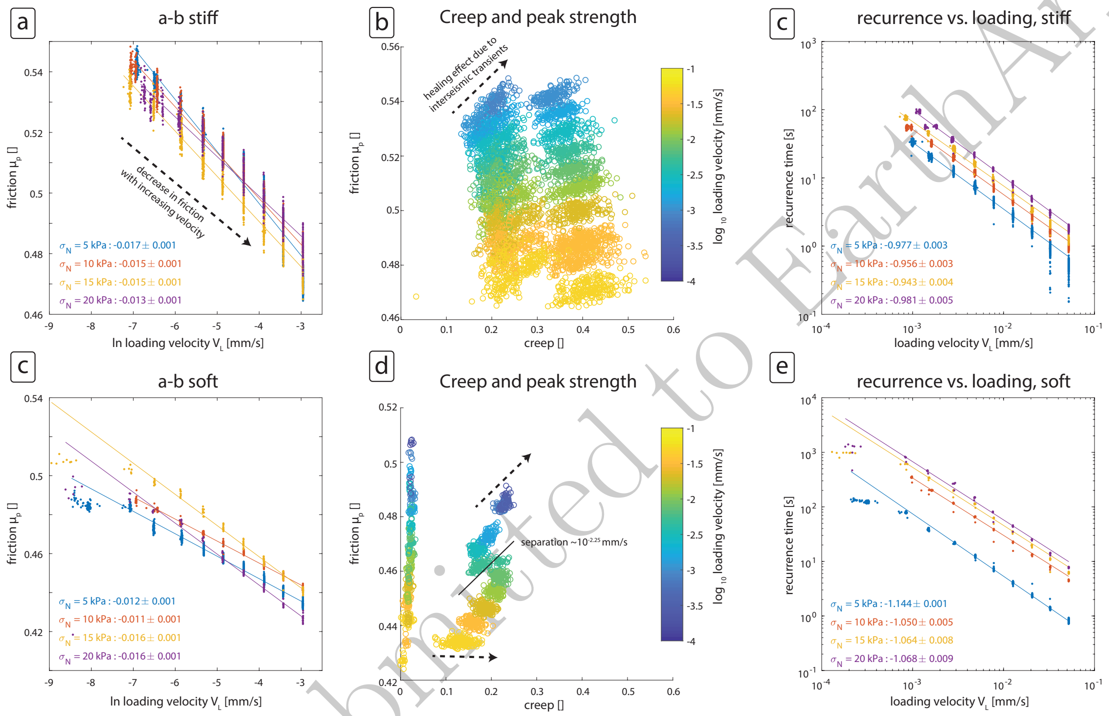

Figure 5: (a+c) Data and scaling of peak friction with loading velocity in the form of $\mu_p \propto (a-b)\, ln(V_L)$. The values given are the parameters (a-b) with the corresponding 2σ confidence interval. (b+d) Effect of creep on peak friction. Higher creep correlates to higher peak friction, for each individual velocity step (color-coded). (c+e) Scaling of recurrence time with loading velocity after **(author?)** [2].

the individual grain scale, such as electrostatic and van-der-Waals forces between the individual glass beads can lead to a certain healing effect. We then also would expect a visible healing effect in the soft system which is not the case. For the soft system we even observe a time-dependent weakening. As a result, the scaling of loading velocity and recurrence has an exponent of $n < -1$.

The major difference between the soft and the stiff system is the amount of creep and the occurrence of precursors. Therefore, we compare the correlation of creep, that includes precursors for the stiff system, and the peak friction at the onset of dynamic failure (Figure 5b+d). We observe an increase in peak friction in the stiff system for each individual loading velocity and normal load (Figure 5b). For the soft system we do not observe a correlation for most normal loads, because there is only a small amount of creep. The experiment with low normal load (#spr5k) does show 10 to 30% creep, but also has the lowest scaling exponent of $n = -1.144$. For high loading velocity ($> 10^{-2.25} \frac{mm}{s}$) the neutral to negative trend is visible (Figure 5d). Below that we suspect a separation (solid line in Figure 5d) because for lower velocities the overall amount of creep drops and we observe an increase in peak friction. Accordingly, we assume that slow creep during the interseismic phase only leads to a small strengthening effect, and that the fault healing is dependent on the loading velocity as was already mentioned by **(author?)** [22]. For the described experiments we think that the precursor slip events have a strong strengthening effect on the experimental fault zone. As a result the evolution of the frictional state ϕ during the interseismic phase is affected by micromechanical rearrangement.

While the scaling of peak friction μ_p with V_L is similar for both systems, we observe that the scaling for final friction μ_e, where the system comes to rest after dynamical failure, is very different for both systems. For the stiff system it is more or less constant for all loading velocities, whereas for the soft system it changes. Therefore, we think that the unloading stiffness of the system plays second order role because it influences the slip distance during an event which is higher for lower unloading stiffness. Consequently, this leads to a different evolution of localization phenomena inside the shear zone, which may weaken the material resulting in $n < -1$.

4.3 Comparison with natural systems

4.3.1 Magnitude size distributions

The magnitude size distribution of natural earthquakes follows the Gutenberg-Richter relation where the cumulative number of events decreases exponentially with increasing magnitude ($\sum N(M) \propto M^{-b}$). Therefore the b-value indicates the relative proportion of small events compared to big events. In the following, we use dynamic stress drop $\Delta\tau$ as a proxy for magnitude. It is linearly related to seismic moment M_0 in our system because σ_N and fault surface A is constant for one experiment:

$$M_0 = \Delta\tau\sigma_N A^{\frac{2}{3}} \tag{5}$$

Seismic moment is then logarithmically related to moment magnitude M_w:

$$M_w = \frac{3}{2}(log_{10}M_0 - 9.1) \tag{6}$$

Experiments with a high stiffness show power law type scaling for the precursory part of the probability distribution with a b-value being smaller than 0.2. In the size interval that is characteristic for the larger main events, the distributions do follow a more Gaussian like behavior and probably shows the stress drop that is characteristic for the fault zone in the ring shear tester. In contrary, for low stiffness the distributions are characterized by power law scaling with $b \approx 1.5$ for normal stresses greater than 5 kPa and $b \approx 2.2$ for experiment #spr5k. The low stiffness distributions more closely follow a G-R type shape with a sudden drop off at larger magnitudes. Where the power law distribution is present, we see that b-value decreases with increasing normal stress. This is in accordance with natural observations, that for highly stressed fault zones the b-value of the earthquake distribution becomes smaller [e.g. 35].

4.3.2 Moment - duration scaling

Another parameter that is frequently obtained for the scaling behavior of earthquakes is the relation of seismic moment and event duration [15, 12]. In general, slip events that grow without bounds within a fault zone show a scaling of $M_0 \propto T^3$ (e.g. earthquakes). In contrast, slip events that span the complete spatial scale of the system and only grow along the fault zone, show a scaling of $M_0 \propto T$ (e.g. slow slip events).

In terms of moment magnitude M_0 - duration T scaling after **(author?)** [15], the precursors cover a very broad range of durations at low magnitude. Therefore, it is not possible to assign a scaling law to them, due to a cross correlation coefficient of 0.02. The cross correlation of $log\, M_0$ and $log\, T$ for the main events is low but reasonable (0.55 - 0.76). The scaling of moment with duration is a power law but with a low goodness of fit for most experiments. Moment scales with duration by $M_0 \propto T^n$ with $n = 0.1$ to 0.3 for experiments without spring and $n = 0.4$ to 0.5 for experiments with spring. This is much smaller than what is observed for natural systems. A possible reason is that the actual duration of an event is much smaller than observed. During the measurement of the unloading stiffness k_u we observed shorter durations using a high-speed camera at 10 kHz. If the actual duration is not linearly related to the measured duration this would increase the power law exponent. Additionally, the definition of earthquake duration is different for natural systems (seismograms) and our model (stress drop duration) which makes it difficult to compare the absolute values.

Furthermore, we consider this a second order feature of our model which may not necessarily be correctly scaled to nature. In order for the analog model to be scaled geometrically it is mandatory to scale the critical slip distance L_c of glass beads to those of fault gouge. Therefore, the total slip during an event is not scaled properly but the model is dynamically similar because the non-dimensionalized dynamic parameter (a-b) is similar.

4.4 Effect of creep on predictability

Although the stick-slip oberserved is highly regular and characteristic, application of simple time and slip predictable recurrence models seem to fail: Comparing the predicted with observed recurrence and observed stress drop for the experiments without spring shows that the majority of points plot away from unity (solid line in Figure 6a+b). As a result, the models for predictability are not able to predict the observed parameters. For lower normal stresses the prediction error increases systematically. The observed recurrences and also stress drops, are up to twice as high as the predictions. For experiments with a spring only the σ_N=5 kPa experiment shows a significant deviation from unity (Figure 6c+d). An increase in normal stress for the low stiffness experiments leads to highly predictable stick-slip events.

However, the recurrence models can be corrected for interseismic creep resulting in a significant improvement of predictions. We observe a direct correlation between forecast error and amount of creep: Events that show a high amount of creep plot close to the dashed lines in figure 6. For 50% creep the observed stress drop is approximately half the size than what is predicted by equation 3. When the predictions are normalized by the amount of creep in the observations, the highest forecast error of -0.60 drops to -0.08 for slip predictability and from 0.38 to 0.07 for time predictability. The normalized predictions still show an increased forecast error for high loading rates.

To summarize, creep at low shear stress retards loading and extends the interseismic phase. i.e. the time until the peak strength is reached. Simple recurrence models tend consequently to overforecast stress drop and underforecast the recurrence time. Because this effect is systematic it should be taken into account when applying simple recurrence models. We interpret the precursory events as being similar to repeating transient events, such as slow slip events, due to their frequent occurrence before a slip event. If the right conditions are met by tuning stiffness, normal stress and loading velocity, the precursors are very regular and can occur multiple times before a main event. When the system is close to the stability boundary in the rate and state framework very subtle perturbations of the system leads to dynamic failure. Furthermore, the regular pattern of the dilation seems to indicate that the granular fault zone does undergo recurring patterns of internal configuration of force chains.

5 Conclusion

We present an experimental setup which is able to generate regular stick slip events in an analog fault gouge to study their dependence on different extrinsic parameters. The slip events reproduce typical characteristics that have been observed in similar experiments in other experimental setups and materials allowing to generalize the observations to natural occurrences of earthquakes. Accordingly, transient phenomena considerably alter the predictability of the slip events and should be taken into account for time-dependent recurrence models of seismic hazard assessment.

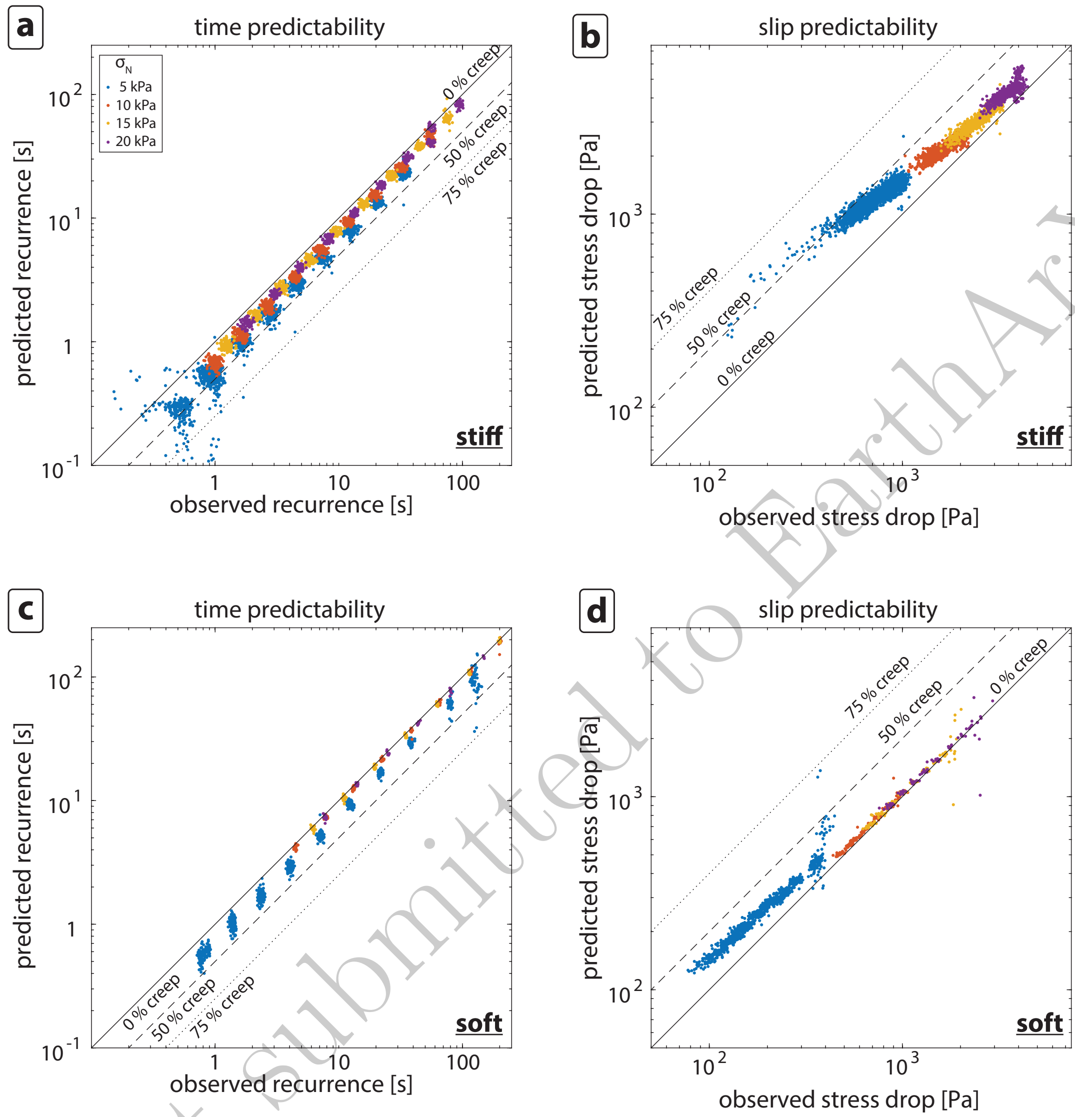

Figure 6: Comparison of predictions and observations from the recurrence and stress drop based models. The dashed lines indicate perfect predictability taking a specified amount of creep into account. (a) Time predictability for experiments with high stiffness. All points plot away from unity which results from the higher amount of creep. (b) Slip predictability at high stiffness shows that the predictions are higher than the observed stress drops with an increasing prediction error with decreasing normal stress. (c) Results for time prediction of the low stiffness experiments. Most slip events lie close to the unity and only the low normal stress experiment shows a stronger shift due to higher creep. (d) The slip predictability also shows that for higher normal stress the slip events are nearly perfectly time slip predictable.

In the experiments, micromechanical rearrangement in the granular package is the major process leading to the observed precursory strengthening and the short period of quiescence before a slip event. The magnitude size distribution of larger events is strongly affected by precursory phenomena and a characteristic scale separation of precursors and larger events is present. We conclude that transients and precursors can strongly affect the statistical characteristics of a single fault zone system.

Acknowledgments

This research has been funded by Deutsche Forschungsgemeinschaft (DFG) through grant CRC 1114 "Scaling Cascades in Complex Systems", Project B01 "Fault networks and scaling properties of deformation accumulation". The experimental data and scripts used to create the figures are available via the GFZ Data Services in **(author?)** [31]. All members of HelTec - "Helmholtz Laboratory for Tectonic Modelling" are acknowledged for their help in the technical realization of this study.

References

[1] Jennifer L Anthony and Chris Marone. Influence of particle characteristics on granular friction. *Journal of Geophysical Research: Solid Earth*, 110(B8), 2005.

[2] NM Beeler, SH Hickman, and T-f Wong. Earthquake stress drop and laboratory-inferred interseismic strength recovery. *Journal of Geophysical Research: Solid Earth*, 106(B12):30701–30713, 2001.

[3] NM Beeler, Terry Tullis, Jenni Junger, Brian Kilgore, and David Goldsby. Laboratory constraints on models of earthquake recurrence. *Journal of Geophysical Research: Solid Earth*, 2014.

[4] Dapeng Bi, Jie Zhang, Bulbul Chakraborty, and Robert P Behringer. Jamming by shear. *Nature*, 480(7377):355–358, 2011.

[5] Charles G Bufe, Philip W Harsh, and Robert O Burford. Steady-state seismic slip–a precise recurrence model. *Geophysical Research Letters*, 4(2):91–94, 1977.

[6] ME Cates, JP Wittmer, J-P Bouchaud, and Ph Claudin. Jamming, force chains, and fragile matter. *Physical review letters*, 81(9):1841, 1998.

[7] F Corbi, F Funiciello, M Moroni, Y Dinther, PM Mai, LA Dalguer, and C Faccenna. The seismic cycle at subduction thrusts: 1. insights from laboratory models. *Journal of Geophysical Research: Solid Earth*, 118(4):1483–1501, 2013.

[8] Deshan Cui, Wei Wu, Wei Xiang, Thiep Doanh, Qiong Chen, Shun Wang, Qingbing Liu, and Jinge Wang. Stick-slip behaviours of dry glass beads in triaxial compression. *Granular Matter*, 19(1):1, 2017.

[9] James H Dieterich. Modeling of rock friction: 1. experimental results and constitutive equations. *Journal of Geophysical Research: Solid Earth*, 84(B5):2161–2168, 1979.

[10] JH Dieterich. Applications of rate-and state-dependent friction to models of fault slip and earthquake occurrence. *Treatise on Geophysics*, 4:107–129, 2007.

[11] B Ferdowsi, M Griffa, RA Guyer, PA Johnson, C Marone, and J Carmeliet. Microslips as precursors of large slip events in the stick-slip dynamics of sheared granular layers: A discrete element model analysis. *Geophysical Research Letters*, 40(16):4194–4198, 2013.

[12] J Gomberg, A Wech, Kenneth Creager, K Obara, and Duncan Agnew. Reconsidering earthquake scaling. *Geophysical Research Letters*, 43(12):6243–6251, 2016.

[13] Ruth A Harris. Large earthquakes and creeping faults. *Reviews of Geophysics*, 55(1):169–198, 2017.

[14] F Heslot, T Baumberger, B Perrin, B Caroli, and C Caroli. Creep, stick-slip, and dry-friction dynamics: Experiments and a heuristic model. *Physical review E*, 49(6):4973, 1994.

[15] Satoshi Ide, Gregory C Beroza, David R Shelly, and Takahiko Uchide. A scaling law for slow earthquakes. *Nature*, 447(7140):76, 2007.

[16] Yao Jiang, Gonghui Wang, Toshitaka Kamai, and Mauri J McSaveney. Effect of particle size and shear speed on frictional instability in sheared granular materials during large shear displacement. *Engineering Geology*, 210:93–102, 2016.

[17] Matthias Klinkmüller, Guido Schreurs, Matthias Rosenau, and Helga Kemnitz. Properties of granular analogue model materials: A community wide survey. *Tectonophysics*, 684:23–38, 2016.

[18] JR Leeman, DM Saffer, MM Scuderi, and C Marone. Laboratory observations of slow earthquakes and the spectrum of tectonic fault slip modes. *Nature communications*, 7, 2016.

[19] Jo Lohrmann, Nina Kukowski, Jürgen Adam, and Onno Oncken. The impact of analogue material properties on the geometry, kinematics, and dynamics of convergent sand wedges. *Journal of Structural Geology*, 25(10):1691–1711, 2003.

[20] Karen Mair, Kevin M Frye, and Chris Marone. Influence of grain characteristics on the friction of granular shear zones. *Journal of Geophysical Research: Solid Earth*, 107(B10), 2002.

[21] C Marone, K Mair, and KM Frye. The effect of particle dimensionality on granular friction: Comparison of laboratory and numerical approaches. In *AGU Fall Meeting Abstracts*, volume 1, page 03, 2002.

[22] Chris Marone. Laboratory-derived friction laws and their application to seismic faulting. *Annual Review of Earth and Planetary Sciences*, 26(1):643–696, 1998.

[23] S Nasuno, A Kudrolli, A Bak, and Jerry P Gollub. Time-resolved studies of stick-slip friction in sheared granular layers. *Physical Review E*, 58(2):2161, 1998.

[24] S Nasuno, A Kudrolli, and Jerry P Gollub. Friction in granular layers: Hysteresis and precursors. *Physical Review Letters*, 79(5):949, 1997.

[25] Kazushige Obara and Aitaro Kato. Connecting slow earthquakes to huge earthquakes. *Science*, 353(6296):253–257, 2016.

[26] James R Rice. Constitutive relations for fault slip and earthquake instabilities. *Pure and applied geophysics*, 121(3):443–475, 1983.

[27] Malte C. Ritter, Karen Leever, Matthias Rosenau, and Onno Oncken. Scaling the sand box - mechanical (dis-) similarities of granular materials and brittle rock. *J. Geophys. Res. Solid Earth*, 2016.

[28] Malte Christian Ritter, Karen Leever, Matthias Rosenau, and Onno Oncken. Supplement to: Scaling the sand box - mechanical (dis-) similarities of granular materials and brittle rock. *GFZ Data Services*, 2016.

[29] Matthias Rosenau, Fabio Corbi, and Stephane Dominguez. Analogue earthquakes and seismic cycles: experimental modelling across timescales. *Solid Earth*, 8(3):597, 2017.

[30] Matthias Rosenau and Onno Oncken. Fore-arc deformation controls frequency-size distribution of megathrust earthquakes in subduction zones. *Journal of Geophysical Research: Solid Earth (1978–2012)*, 114(B10), 2009.

[31] M. Rudolf, M. Rosenau, and O. Oncken. Supplement to: Interseismic deformation transients and precursory phenomena: Insights from spring-slider experiments with a granular fault zone. *GFZ Data Services*, 2017.

[32] Andy Ruina. Slip instability and state variable friction laws. *Journal of Geophysical Research: Solid Earth*, 88(B12):10359–10370, 1983.

[33] Christopher H Scholz. Earthquakes and friction laws. *Nature*, 391(6662):37–42, 1998.

[34] D Schulze. Development and application of a novel ring shear tester. *Aufbereitungs Technik*, 35(10):524–535, 1994.

[35] Bernd Schurr, Günter Asch, Sebastian Hainzl, Jonathan Bedford, Andreas Hoechner, Mauro Palo, Rongjiang Wang, Marcos Moreno, Mitja Bartsch, Yong Zhang, et al. Gradual unlocking of plate boundary controlled initiation of the 2014 iquique earthquake. *Nature*, 512(7514):299–302, 2014.

[36] Kunihiko Shimazaki and Takashi Nakata. Time-predictable recurrence model for large earthquakes. *Geophysical Research Letters*, 7(4):279–282, 1980.

[37] Terry E Tullis and John D Weeks. Constitutive behavior and stability of frictional sliding of granite. In *Friction and faulting*, pages 383–414. Springer, 1986.